Momentum balances on the inner continental shelf at Martha's Vineyard Coastal Observatory

Melanie R. Fewings[1,2] and Steven J. Lentz[3]

Received 22 June 2009; revised 9 June 2010; accepted 7 September 2010; published 9 December 2010.

[1] The subtidal, depth-average momentum balances in 12 m and 27 m water depth are investigated using observations from 2001 to 2007 of water velocity, temperature, and density; bottom pressure; surface gravity waves; and wind stress. In the fluctuating across-shelf momentum budget, the dominant terms are surface wind stress, pressure gradient, and Coriolis acceleration. The balance is a combination of (1) the geostrophic balance expected at midshelf sites and (2) the coastal setup and setdown balance driven by the across-shelf wind stress expected where surface and bottom boundary layers overlap. At the 12 m site, the estimated wave radiation stress gradient due to surface gravity wave shoaling is also large but is uncorrelated with the observed pressure gradient. A simple model suggests the wave radiation stress gradient is balanced by an across-shelf pressure gradient with a spatial scale too small to resolve with this mooring array. In the fluctuating along-shelf momentum balance, the dominant terms are surface wind stress, pressure gradient, and bottom stress at the shallower site, but the other estimated terms are not negligible. Our results support the Grant and Madsen (1986) formulation for wave-induced bottom stress. The fluctuating along-shelf pressure gradient is mainly a local sea level response to wind forcing, not a remotely generated pressure gradient. A strong correlation between along-shelf velocity and along-shelf wind stress at the shallower site is captured by a simple steady model of imbalance between wind stress and pressure gradient balanced by linear bottom drag.

Citation: Fewings, M. R., and S. J. Lentz (2010), Momentum balances on the inner continental shelf at Martha's Vineyard Coastal Observatory, *J. Geophys. Res.*, *115*, C12023, doi:10.1029/2009JC005578.

1. Momentum Balances on the Continental Shelf

[2] The inner continental shelf, where the water is tens of meters deep, is a transition region between the surfzone and the midshelf. The surfzone is where breaking waves dominate the dynamics. The midshelf is where the frictional surface and bottom boundary layers are well separated and thin relative to the water depth, and an interior geostrophic region exists. In the inner shelf transition region, the momentum balance may contain elements of both the surfzone balance and the midshelf balance. The inner shelf has been defined as the region outside the surfzone where the surface and bottom boundary layers overlap [*Lentz*, 1995], where the boundary layers interact [*Li and Weisberg*, 1999b], or where the boundary layers occupy a substantial fraction of the water column and a cross-shelf divergence in the Ekman layer transports exists [*Weisberg et al.*, 2001].

[3] The across-shelf momentum balance over the inner shelf can be a complex superposition of three balances. The first, a geostrophic balance between the Coriolis acceleration and the across-shelf pressure gradient, tends to dominate the across-shelf momentum balance farther offshore, at midshelf [*Allen and Kundu*, 1978; *Brown et al.*, 1985, 1987; *Thompson and Pugh*, 1986; *Noble and Butman*, 1983; *Lee et al.*, 1984, 1989; *Lentz et al.*, 1999; *Shearman and Lentz*, 2003; *Liu and Weisberg*, 2005]. The second, a wave setup balance between the wave radiation stress divergence and the across-shelf pressure gradient, tends to dominate farther onshore, in the surfzone [*Longuet-Higgins and Stewart*, 1964; *Bowen et al.*, 1968; *Lentz and Raubenheimer*, 1999; *Raubenheimer et al.*, 2001]. Both those balances can be important over the inner shelf [*Lentz et al.*, 1999]. The third, a coastal setup or setdown balance between the across-shelf wind stress and the across-shelf pressure gradient, has also been shown to be important, both observationally [*Blanton*, 1981; *Lee et al.*, 1989; *Lentz et al.*, 1999; *Liu and Weisberg*, 2005] and in numerical modeling studies [*Li and Weisberg*, 1999a, 1999b; *Tilburg*, 2003] due to the shallowness of the water, relative to the surface and bottom boundary layer thicknesses. In the surface and bottom boundary layers, vertical stress divergences due to wind and bottom stress are dominant terms in the momentum balance; over the inner shelf, those boundary

[1] MIT/WHOI Joint Program in Oceanography, Applied Ocean Science and Engineering, Woods Hole, Massachusetts, USA.
[2] Now at Marine Science Institute, University of California, Santa Barbara, California, USA.
[3] Department of Physical Oceanography, Woods Hole Oceanographic Institution, Woods Hole, Massachusetts, USA.

Copyright 2010 by the American Geophysical Union.
0148-0227/10/2009JC005578

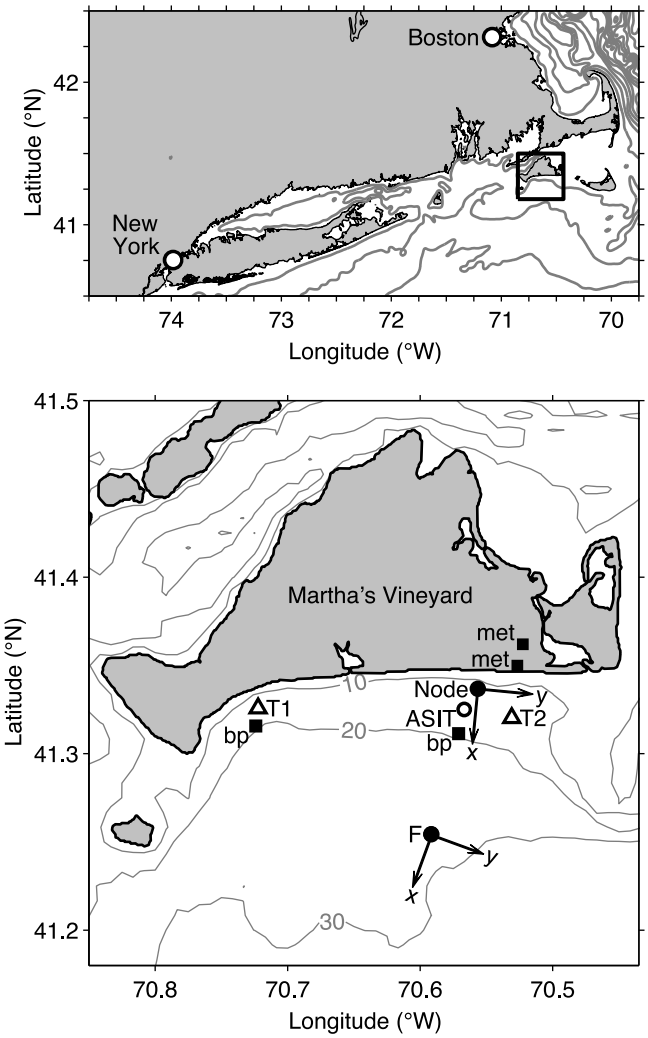

Figure 1. (top) Location of study area. The Middle Atlantic Bight extends from Cape Cod south to Cape Hatteras. Isobaths are shown in increments of 20 m (i.e., the 20, 40, and 60 m isobaths). (bottom) Study area. Isobaths are labeled in m. Solid circles are MVCO Node and mooring F from CBLAST 2003 and SWWIM I. Triangles are moorings T1 and T2, deployed during CBLAST 2003 only. Open circle is MVCO air-sea interaction tower (ASIT). Squares on land are MVCO meteorological masts. Squares ("bp") near 20 m isobath is bottom pressure measurements in 2001.

layers often fill the entire water column. Each of the three balances is between the across-shelf pressure gradient and a different other term. The dynamics of the inner shelf are complicated because the across-shelf pressure gradient may be simultaneously balanced by one, two, or all three of those other terms [e.g., *Lentz et al.*, 1999].

[4] The along-shelf momentum balance over the inner shelf may be simpler than at midshelf, where the Coriolis, wind stress, bottom stress, acceleration, and pressure gradient terms can all be important [*Allen and Smith*, 1981; *Lentz and Winant*, 1986; *Lee et al.*, 1984, 1989]. Over the inner shelf, the balance tends to be between three terms: along-shelf wind stress and bottom stress and pressure gradient [*Scott and Csanady*, 1976; *Pettigrew*, 1981; *Lentz and Winant*, 1986; *Masse*, 1988; *Lee et al.*, 1989; *Lentz*, 1994]. In the surfzone, the wave radiation stress gradient becomes a dominant term and is balanced by bottom stress [*Thornton and Guza*, 1986; *Svendsen and Putrevu*, 1994; *Feddersen et al.*, 1998; *Lentz et al.*, 1999]. Few previous studies have considered wave radiation stress over the inner shelf [*Lentz et al.*, 1999].

[5] Here, terms in the across-shelf and along-shelf depth-average momentum budgets are estimated at sites in 12 and 27 m water depth near the Martha's Vineyard Coastal Observatory (MVCO) in Massachusetts to determine the dominant dynamical balances in the water column over the continental shelf. Under the typical wind and stratification conditions for this area, estimated surface boundary layer thicknesses indicate the MVCO site is dynamically within the inner shelf [*Fewings et al.*, 2008]. The regional circulation has been described by, e.g., *Beardsley et al.* [1985]. Our previous studies at MVCO describe the cross-shelf circulation driven by surface gravity waves [*Lentz et al.*, 2008] and across-shelf wind [*Fewings et al.*, 2008]. Below, section 2 describes the observations. Section 3 presents the momentum balance equations and explains how we estimated the terms. Section 4.1 describes the dominant across-shelf balances, in which the pressure gradient, across-shelf wind, Coriolis, and wave radiation stress gradient terms are all important. Section 4.2 describes the dominant along-shelf balances, which involve the pressure gradient, along-shelf wind stress, bottom stress, and Coriolis terms, though the acceleration term is not completely negligible either. In section 5 we discuss the expected form of the across-shelf sea level slope during wind forcing, wave forcing, and geostrophic balance; compare the relative sizes of the across- and along-shelf pressure gradients; examine the dynamics behind a strong correlation of along-shelf wind and along-shelf flow; and examine which wind angle gives the strongest response in along-shelf flow. In section 6 we summarize the main results and give some recommendations for future studies.

2. Observations

[6] The data are from four sources. The first data set is the Martha's Vineyard Coastal Observatory time series of water velocity, wind velocity, and water column bottom pressure, which extends from 2001 to 2007 at the 12 m Node site (Figure 1). The second data set is the Coupled Boundary Layers Air-Sea Transfer in Low Winds (CBLAST-Low) measurements from July to October 2003 of water temperature, velocity, salinity, and, bottom pressure. The third data set is from the Stratification, Wind and Waves on the Inner Shelf at MVCO (SWWIM I) experiment, which included measurements of water velocity, temperature, salinity, and bottom pressure during December 2004 to May 2005. The second and third data sets include measurements at the Node and site F on the 27 m isobath, and are described in more detail by *Fewings* [2007] and *Fewings et al.* [2008]. The fourth data set is a time series of bottom pressure measurements on the 19 m isobath obtained in June–August during CBLAST 2001. The mooring locations are shown in Figure 1. Measurements are available of the along-shelf pressure gradient mainly in summer, during June–August 2001 and July–October 2003; and of the across-shelf pressure gradient during July–October 2003 and December 2004 to May 2005. For brevity

we focus on times when pressure gradient estimates are available, although the other terms estimated from the MVCO time series are available from 2001 to 2007 and those data are included in analyses that do not involve the pressure gradient. The time resolution of all the data used here is 20 min, though the sampling rate of most instruments was substantially faster (for details, see *Fewings* [2007]).

3. Calculation of Momentum Budget Terms From Observations

[7] The depth-averaged across-shelf momentum balance equation, following *Lentz et al.* [1999] but neglecting nonlinear advection and including the *Hasselmann* [1970] wave stress term, is

$$\frac{\partial \overline{u}}{\partial t} = f\overline{v} + f\overline{v}_{st} - \frac{1}{\rho_0 h}\int_{-h}^{0}\frac{\partial p}{\partial x}\,dz + \frac{\tau_s^x - \tau_b^x}{\rho_0 h} - \frac{1}{\rho_0 h}\left(\frac{\partial S^{xx}}{\partial x} + \frac{\partial S^{yx}}{\partial y}\right) \tag{1}$$

and the along-shelf momentum equation is

$$\frac{\partial \overline{v}}{\partial t} = -f\overline{u} - f\overline{u}_{st} - \frac{1}{\rho_0 h}\int_{-h}^{0}\frac{\partial p}{\partial y}\,dz + \frac{\tau_s^y - \tau_b^y}{\rho_0 h} - \frac{1}{\rho_0 h}\left(\frac{\partial S^{xy}}{\partial x} + \frac{\partial S^{yy}}{\partial y}\right), \tag{2}$$

where all variables are averaged over many wave periods, $\mathbf{u} = (u, v)$ is the horizontal velocity vector, $z = 0$ is the mean water level over each deployment, $z = -h(x)$ is the bottom, an overbar indicates depth average, f is the Coriolis parameter, ρ_0 is the density of seawater, p is pressure, $\mathbf{u}_{st} = (u_{st}, v_{st})$ is the Stokes drift velocity [*Stokes*, 1847], $\boldsymbol{\tau}_{s,b}$ are the surface (wind) and bottom stresses, and $\partial S^{xx}/\partial x$ and similar terms are the wave radiation stresses [e.g., *Longuet-Higgins and Stewart*, 1964]. The derivation of the *Hasselmann* [1970] wave radiation stress terms ($f\overline{v}_{st}$ and $f\overline{u}_{st}$) that are due to the interaction of surface gravity waves with Earth's rotation is given by, e.g., *Xu and Bowen* [1994].

[8] All the momentum budget terms estimated below are low-pass filtered with a $(33\ \mathrm{h})^{-1}$ cutoff to remove tidal and other high-frequency variations (for details, see *Fewings* [2007]). The coordinate system at each mooring is based on the principal axis directions of the subtidal (i.e., low-pass filtered) depth-average velocity, with x positive offshore and y positive along-shelf eastward (Figure 1).

[9] Wind stress was calculated using the *Smith* [1988] bulk formula and adjusted as described by Appendix A of *Fewings* [2007]. For the acceleration, Coriolis, and other terms, we used centered differences to calculate derivatives and a constant value to extrapolate vertically to the surface and bottom; the results presented here do not change substantially if a linear extrapolation is used instead. We used the National Geophysical Data Center high-resolution bathymetry (http://www.ngdc.noaa.gov) interpolated onto a 50 m grid for $h(x)$.

3.1. Bottom Stress

[10] To estimate bottom stress at each site we used a quadratic drag formula

$$\boldsymbol{\tau}_b = -\rho_0 C_d |\mathbf{u}_b|\,\mathbf{u}_b, \tag{3}$$

where $\mathbf{u}_b$ is the observed velocity 3 m above bottom. The drag coefficient $C_d = 1.45 \times 10^{-3}$ was estimated at the 12 m site from comparison of the unfiltered $\mathbf{u}_b$ with a stress estimate based on turbulent covariance measurements [*Lentz*, 2008, Figure B1; J. Trowbridge, personal communication, 2006]. Direct covariance stress estimates from the Node ADCP also yield $C_d \sim 1.5 \times 10^{-3}$ [*Kirincich et al.*, 2010]. We used the same C_d for the 27 m site.

[11] Wave-current interactions are thought to enhance bottom stress in water depths $O(10\ \mathrm{m})$ [e.g., *Grant and Madsen*, 1979]. To test the hypothesis that wave-enhanced bottom friction would improve closure of the momentum budget at the 12 m site, we estimated a bottom stress $\tau_{b,GM}$ using the *Grant and Madsen* [1986] formulation, with a roughness height $z_0 = 1.2 \times 10^{-4}$ m derived from the same turbulent covariance measurements (J. Trowbridge, personal communication, 2006). We refer to this as the GM bottom stress.

3.2. Pressure Gradients

[12] The pressure gradient terms in equations (1) and (2) can be written as the sum of (1) the gradient of bottom pressure p^b and (2) a term due to density variations [*Brown et al.*, 1985]; for the across-shelf direction

$$\frac{1}{h}\int_{-h}^{\eta}\frac{\partial p}{\partial x}\,dz = \frac{\partial p^b}{\partial x} + \frac{1}{h}\frac{\partial}{\partial x}\int_{-h}^{\eta} g\rho z\,dz, \tag{4}$$

where we assume $\eta \ll h$, and similarly for the along-shelf equation. The mean bottom pressure gradient is not accurately known from the observations, so we remove the mean measured bottom pressure gradient from each deployment and consider only time variations about the mean, following previous studies [e.g., *Brown et al.*, 1985; *Lentz et al.*, 1999].

[13] To estimate the along-shelf bottom pressure and density gradients, during CBLAST 2003 we used moorings T1 and T2 on the 15 m isobath (Figure 1). The middepth temperature and near-bottom conductivity sensors failed on T1 so only the near-surface density gradient is available. During CBLAST 2001, we used the sensors labeled "bp" in Figure 1 when available, and a third sensor deployed ~15 km farther east on the same isobath (not shown) to fill in the bottom pressure gradient during times when bottom pressure from the eastern bp sensor was not available. The along-shelf pressure gradient measured between the sensors farther apart was similar to, but smaller in magnitude than, the gradient between the bp sensors.

[14] To estimate the across-shelf bottom pressure gradient and across-shelf density gradient during CBLAST 2003 and SWWIM I, we used the Node and F moorings. Density information was available throughout the water column at the Node and F during CBLAST 2003, and at F and near surface at the Node during SWWIM I.

[15] The density contribution to the pressure gradient was only 3–6% of the gradient of bottom pressure, in both the along-shelf and across-shelf directions, as measured by the standard deviations on subtidal time scales of the terms on the right-hand side of equation (4) and the equivalent terms for the along-shelf direction [see also *Fewings*, 2007, Figure 3-2]. This is in contrast to midshelf [*Lentz et al.*, 1999; *Shearman and Lentz*, 2003] and an inner shelf site influenced by a river outflow plume [*Lentz et al.*, 1999] where the baroclinic pressure gradient can be the

same size as the barotropic pressure gradient. Consequently, we used the bottom pressure gradient to represent the full pressure gradient when density measurements were not available.

3.3. Wave Terms

[16] Typical significant wave heights at MVCO are 0.5–3 m (Figure 2), and dominant wave periods are 4–10 s. We estimated $f\overline{\mathbf{u}}_{st}$ from the Stokes drift [*Longuet-Higgins*, 1953] as

$$f\overline{\mathbf{u}}_{st}(t) = f\frac{gH_{sig}^2}{16ch}\hat{\mathbf{k}}, \tag{5}$$

where c is the wave phase speed and $\hat{\mathbf{k}}$ is a unit wave vector.

[17] We estimated S^{xx} from *Longuet-Higgins and Stewart* [1964] as

$$S^{xx} = E\left[\frac{c_g}{c}\left(1+\cos^2\theta_w\right) - \frac{1}{2}\right], \tag{6}$$

where $E = g\rho_0 H_{sig}^2/16$ is the wave energy; $\mathbf{c}_g$ is the magnitude of the group velocity; and θ_w is the direction of wave propagation, measured counterclockwise from the $+x$ direction, so $\theta_w = 180°$ for waves going directly onshore.

[18] To calculate c and $\mathbf{c}_g$, we used the observed dominant wave period and linear wave theory. We used conservation of wave energy flux $\mathbf{c}_g E$, assuming no dissipation of surface gravity wave energy, and Snell's law to estimate H_{sig} and θ_w on the 11 and 13 m isobaths from H_{sig} and θ_w observed at the 12 m isobath. To calculate the across-shelf gradient of S^{xx}, we estimated S^{xx} on the 11 and 13 m isobaths and used a finite difference approximation.

[19] We assume S_x^{yx} is negligible since the MVCO Node site is always outside the surfzone [*Lentz et al.*, 2008] and we are assuming no wave dissipation. S_y^{xy} and S_y^{yy} cannot be estimated from these observations.

4. Observed Momentum Balances

4.1. Across-Shelf Momentum Budget

[20] To measure the size of each term in the fluctuating momentum budget, we used the standard deviation on subtidal time scales. In the across-shelf budget, the dominant terms are the wind stress, pressure gradient, and Coriolis acceleration (Figure 2 and Table 1). The other terms are an order of magnitude smaller, except the wave radiation stress gradient at the 12 m site (addressed below). The same four terms dominated in an observed momentum budget at 13 m depth on the North Carolina inner shelf [*Lentz et al.*, 1999]. The across-shelf wind stress and wave radiation stress terms are smaller at the 27 m site than at the 12 m site due to the dependence of those terms on h^{-1}. Below, we focus on the dominant fluctuating terms.

[21] To determine which terms in the momentum budget balance each other, we calculated correlation coefficients between the pressure gradient and the other dominant terms (Table 2). We averaged each term over the 12 and 27 m sites because the pressure gradient estimate is most appropriate for the point midway between those sites. The across-shelf pressure gradient is balanced by both wind stress and Coriolis acceleration: that combination of terms gives the highest correlation (Table 2 and Figures 2e and 3). Adding other terms to the combinations shown in Table 2 does not improve the correlation.

[22] In spite of the large size of the estimated wave radiation stress gradient at the 12 m site (Table 1), it is not significantly correlated with the estimated across-shelf pressure gradient (Figures 2d and 2e). Either (1) the estimated wave radiation stress gradient is an overestimate or (2) the across-shelf pressure gradient is an underestimate of the true gradient at the 12 m site during wave forcing. A simple model (section 5.1) indicates the pressure gradient due to wave-driven set down likely exists over a small across-shelf scale and is not resolved by these observations, supporting the point 2. Compared to the wave forcing, the wind forcing and Coriolis acceleration have larger cross-shelf scales and are resolved by the pressure sensors. We do not include the wave radiation stress term in the closure analysis below.

[23] To test whether the momentum budget closes, we calculated the regression slope between the dominant terms, again averaging over the 12 and 27 m sites (Table 2). The slope of wind stress plus Coriolis acceleration versus pressure gradient is equal to 1 within the uncertainty of the measurements. The fluctuating across-shelf momentum budget does close with only those three terms (Figures 2e and 3).

[24] Since this is a linear balance, it is convenient to think of the pressure gradient as the linear combination of three pressure gradients, each generated in response to a different term (Coriolis, wind stress, and wave radiation stress gradient). These observations capture the first two pressure gradients. Then the across-shelf momentum balance is the superposition of two or three separate balances: geostrophic balance (Figure 4a), coastal setup driven by the cross-shelf wind stress (Figure 4b), and possibly wave setdown outside the surfzone due to the wave radiation stress gradient associated with shoaling waves (Figure 4c).

[25] Although the bottom stress is not a dominant term (its magnitude is ~10–20% of the wind stress), the wind stress and bottom stress are significantly negatively correlated at both the 12 and 27 m sites. The strong inverse relation between τ_s^x and τ_b^x at the 12 m site (correlation coefficient $r = -0.7$, with or without GM bottom stress) is consistent with a two-layer across-shelf flow structure driven by across-shelf wind forcing observed at that site [*Fewings et al.*, 2008]. When the wind is directed offshore, the near-surface flow is offshore and there is an onshore return flow near the bottom, leading to a negative value for τ_b^x.

[26] In the time-mean budget, the wind stress is near zero (Table 1). At the 12 m site, the wave radiation stress term is largest, followed by Coriolis acceleration. At the 27 m site, the Coriolis term is largest. Though the mean sea level gradient cannot be accurately measured, the residual can be interpreted as due to the mean across-shelf sea level gradient. The observed residual (including all terms) combined with the hydrostatic relation indicates the mean sea level gradient $\partial\eta/\partial x$ is $0–3 \times 10^{-7}$ at the 12 m site (depending on whether times with no pressure gradient measurements are included) and $\sim -5 \times 10^{-7}$ at the 27 m site. This is consistent with sea level decreasing from the 12 m site toward shore due to a wave setdown balance dominating over geostrophy, and sea level decreasing from the 27 m site toward deeper water

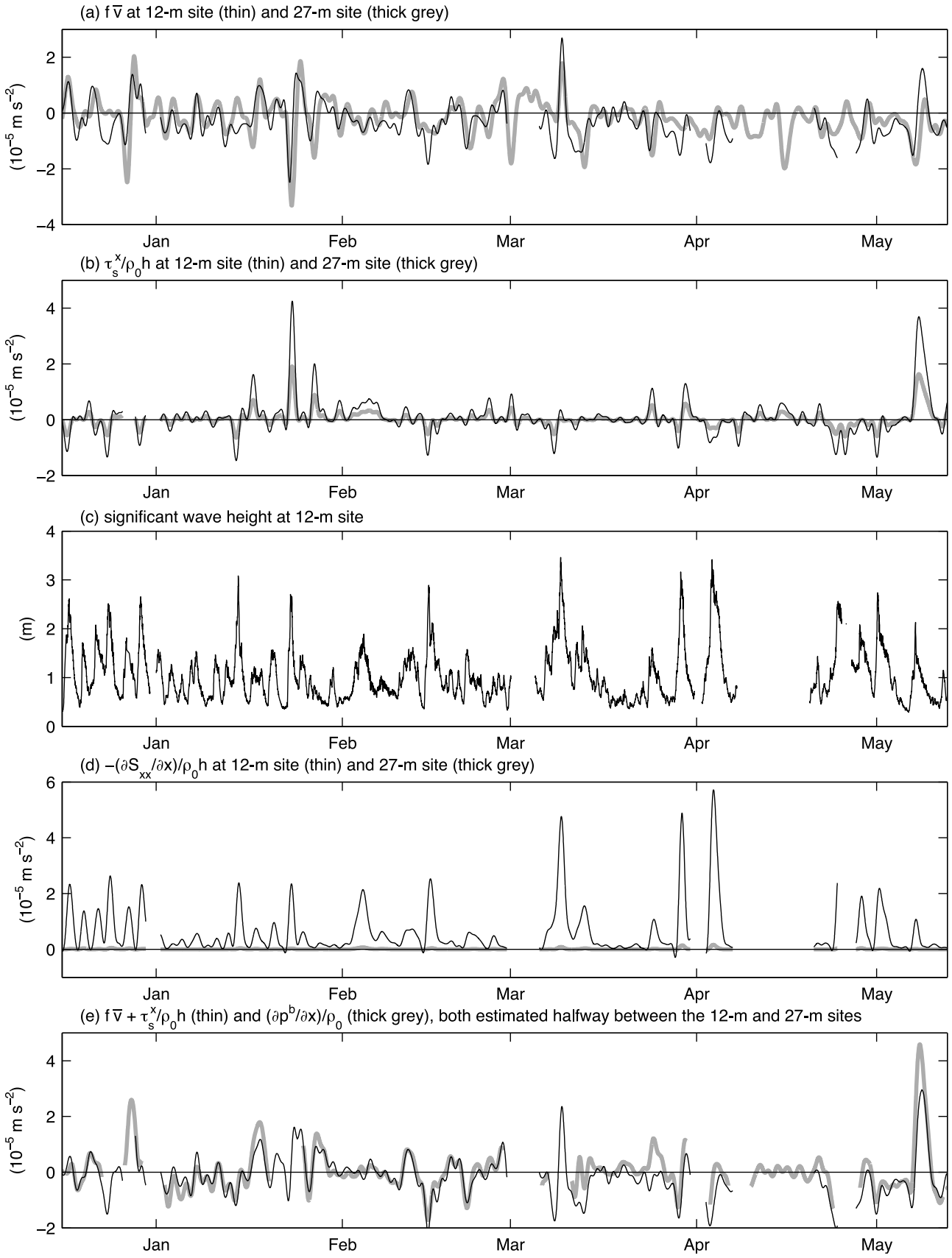

Figure 2. (a–e) Dominant terms in subtidal across-shelf momentum budget during SWWIM I (2004–2005) and (c) unfiltered significant wave height at the 12 m site.

Table 1. Statistics of Terms in the Across- and Along-Shelf Momentum Budgets at the 12 and 27 m Sites, During Times When Estimates of All Terms are Available[a]

	Across			Along		
	Term	12 m	27 m	Term	12 m	27 m
Wind stress	$\frac{\tau_s^x}{\rho_0 h}$	5	2	$\frac{\tau_s^y}{\rho_0 h}$	2	1
Wave radiation stress gradient	$-\frac{1}{\rho_0 h}\frac{\partial S^{xx}}{\partial x}$	7	0.2			
Pressure gradient	$-\frac{1}{\rho_0}\frac{\partial p^b}{\partial x}$	6	6	$-\frac{1}{\rho_0}\frac{\partial p^b}{\partial y}$	2	2
Coriolis	$f\overline{v}$	5	7	$-f\overline{u}$	1	2
Bottom stress	$-\frac{\tau_b^x}{\rho_0 h}$	0.3	0.2	$-\frac{\tau_b^y}{\rho_0 h}$	1	0.3
GM bottom stress	$-\frac{\tau_{b,GM}^x}{\rho_0 h}$	0.7	–	$-\frac{\tau_{b,GM}^y}{\rho_0 h}$	2	–
Hasselmann wave stress	$f\overline{v}_{st}$	0.3	0.1	$-f\overline{u}_{st}$	0.5	0.2
Acceleration	$\frac{\partial \overline{u}}{\partial t}$	0.2	0.3	$\frac{\partial \overline{v}}{\partial t}$	1	1

[a]Units are 10^{-6} m s^{-2}.

due to a geostrophic balance with the mean westward along-shelf flow [*Lentz*, 2008].

4.2. Along-Shelf Momentum Budget

[27] The largest terms in the fluctuating along-shelf momentum budget at the 12 m site are pressure gradient, wind stress, and bottom stress if we use the GM formulation (Figure 5 and Table 1). The Coriolis and acceleration terms (and bottom stress if not using GM) are not negligible; they are about half as large as the dominant terms. At the 27 m site, the pressure gradient and Coriolis terms are largest but wind stress and acceleration are not negligible either. The previous statements are based on times when along-shelf pressure gradient measurements are available, mainly in summer. If we consider all times including winters, when pressure gradient measurements are not available, every along-shelf term in Table 1 except Coriolis is simply twice as large.

[28] During summer, when along-shelf pressure gradient measurements are available, the pressure gradient is significantly correlated with the wind stress at both the 12 m and 27 m sites (Table 3). The wind and bottom stresses are weak and not significantly correlated in summer. Nevertheless, the pressure gradient is significantly correlated with the difference between wind stress and bottom stress at each site, suggesting the measured along-shelf pressure gradient is fairly accurate and does help to close the momentum balance.

[29] Calculating the correlation of pressure gradient with other terms at each site assumes the along-shelf pressure gradient is constant in the across-shelf direction. To more accurately compare the wind stress term $\tau_s^y/\rho_0 h$ with the pressure gradient term $(\partial p^b/\partial y)/\rho_0$ in the MVCO area, we used for h the water depth at which the pressure gradient was measured: 19 m in 2001 and 15 m in 2003 (Table 4). The along-shelf pressure gradient is significantly correlated with the along-shelf wind stress at zero lag, with a slope near 1 and an intercept not significantly different from zero (Figure 6). The maximum lagged correlations are not significantly different from the correlations at zero lag, indicating the along-shelf wind stress and along-shelf pressure gradient are essentially in phase in time. This suggests the fluctuating along-shelf pressure gradient is largely a response to local wind forcing, rather than being a remotely generated pressure gradient.

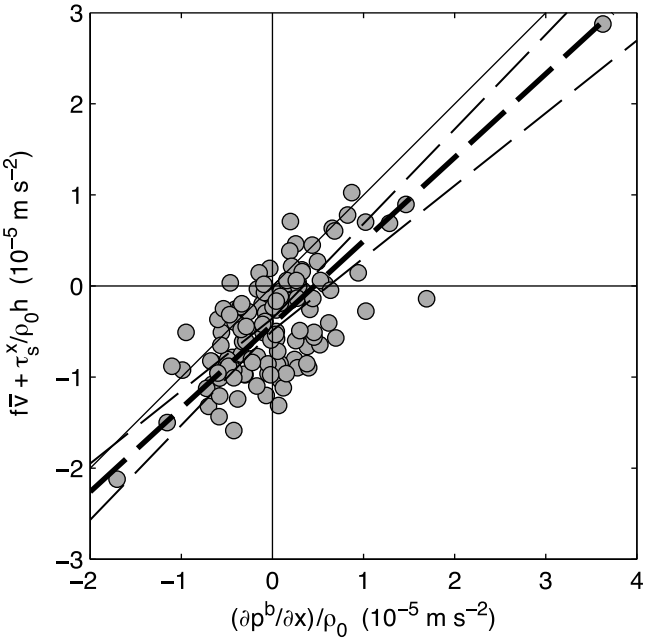

Figure 3. Comparison of Coriolis plus wind stress versus pressure gradient term in the across-shelf momentum budget. The Coriolis and wind stress terms have been averaged between the 12 and 27 m sites. Solid line has slope 1. Thick dashed line is a best-fit line, with 95% confidence intervals as thin dashed lines. Grey symbols show 33 h low-pass filtered ("subtidal") data subsampled every 33 h. See Table 2 for regression slope and correlation coefficient. If the across-shelf momentum budget closed exactly with the terms plotted, the best-fit line (dashed) would lie on the solid line.

[30] At the 12 m site, the regression slope of wind stress against pressure gradient is close to 1 (Table 3). Including the substantial bottom stress term results in a budget that closes just as well. Including the acceleration term improves the regression slope against pressure gradient slightly but not significantly, suggesting a four-way balance between acceleration, pressure gradient, wind stress, and bottom stress may be important (though see section 5.3). Including other terms does not improve the regression against pressure gradient. The primary along-shelf balance during times when we have measurements of the pressure gradient is between wind stress, pressure gradient, and bottom stress, and the budget closes with those three terms.

[31] When we include times with strong winter forcing (when no pressure gradient measurements are available), at the 12 m site the along-shelf wind stress and bottom stress

Table 2. Regression Slope and Correlation Coefficient r of Terms in the Across-Shelf Momentum Budget Against $(\partial p^b/\partial x)/\rho_0$ With Zero Lag, for Times When All Terms are Available[a]

	Slope	r
$f\overline{v}$	1.1 ± 0.1	0.5
$\frac{\tau_s^x}{\rho_0 h}$	0.5 ± 0.1	0.7
$f\overline{v} + \frac{\tau_s^x}{\rho_0 h}$	0.8 ± 0.2	0.7

[a]All correlation coefficients reported in this manuscript are significant at the 95% confidence level.

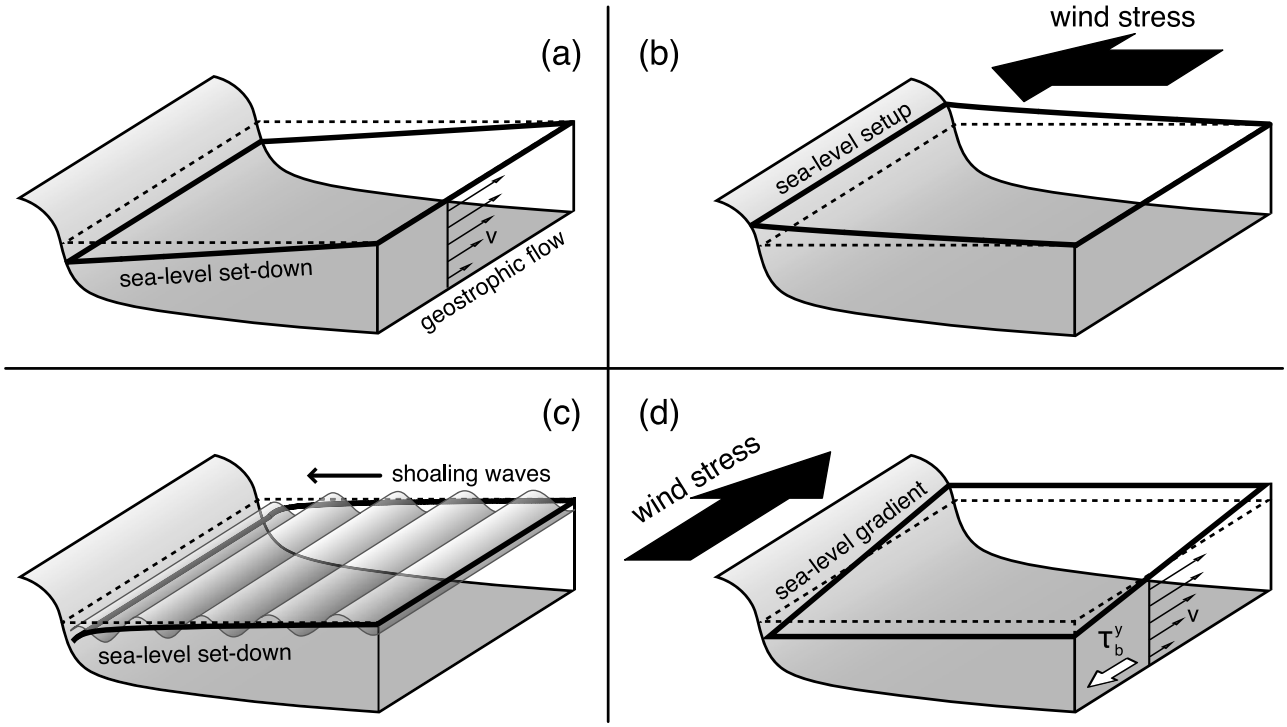

Figure 4. Schematics of dominant subtidal momentum balances over the inner continental shelf: across-shelf (Figures 4a–4c) and along-shelf (Figure 4d). Dashed lines indicate undisturbed sea level in each case. (a) Geostrophic balance between an eastward along-shelf flow v and the across-shelf pressure gradient due to lower sea level at the coast compared to offshore. If the along-shelf flow were westward, the sea level would be raised at the coast. (b) Across-shelf wind driven coastal setup. An onshore wind stress balances the across-shelf pressure gradient associated with raised sea level at the coast. For an offshore-ward wind stress, the coastal sea level would instead be setdown. (c) Wave-driven coastal setdown. Shoaling of the waves due to decreasing bottom depth causes a divergence in the wave radiation stress that is balanced by lowered sea level near the coast. The surfzone, where there is coastal setup due to breaking waves, is not shown. Note the balance in Figure 4c was not observed but is inferred at the 12 m site due to the large calculated wave radiation stress gradient. Probably the pressure sensors were not deployed close enough together to capture the sea level setdown. (d) The along-shelf wind stress term $\tau_s^y/\rho_0 h$ balances the along-shelf pressure gradient term $-(\partial p^b/\partial y)/\rho_0$. At this site, along-shelf wind stress is associated with increasing sea level in the direction of the wind stress, probably due to topography upstream. The sea level gradient produces a bottom pressure gradient in the along-shelf direction. The bottom stress τ_b^y due to the along-shelf flow v also contributes to the momentum balance. The along-shelf flow v is driven by the time-varying imbalance between the pressure gradient and wind stress terms.

are well correlated ($r = 0.8$), in contrast to the summer case above. The regression slope of bottom stress against wind stress over all times is order 1, indicating the primary along-shelf balance at the 12 m site during strong winter forcing is between wind and bottom stress. The slope equals 1.0 when we use the GM bottom stress formulation, closing the budget with wind and bottom stress alone and supporting the form hypothesized by *Grant and Madsen* [1986] for wave-enhanced bottom stress. At the 27 m site, the relation of wind and bottom stress is less strong: $r = 0.5$ and slope = 0.35. The bottom stress, due to its dependence on $1/h$, is less important for balancing the wind stress at the 27 m site. Still, the observed relation between bottom stress and wind stress is stronger at both sites than at the Coastal Mixing and Optics experiment site on the 70 m isobath south of MVCO, where the bottom stress is ~7 times weaker than the wind stress [*Shearman and Lentz*, 2003].

[32] The results at the 12 m site are similar to previous inner-shelf studies in that along-shelf wind stress and along-shelf pressure gradients are the dominant driving mechanisms for along-shelf flow, with bottom stress an important part of the response [e.g., *Scott and Csanady*, 1976; *Pettigrew*, 1981; *Lentz and Winant*, 1986; *Masse*, 1988; *Lee et al.*, 1989; *Lentz*, 1994; *Lentz et al.*, 1999; *Liu and Weisberg*, 2005]. The acceleration and Coriolis terms have also been found important in previous midshelf studies [e.g., *Allen and Smith*, 1981; *Lee et al.*, 1984, 1989; *Lentz et al.*, 1999; *Liu and Weisberg*, 2005].

[33] At the 27 m site, the budget does not close with wind stress and pressure gradient alone, and including the Coriolis (not shown) and/or acceleration terms does not improve the closure (Table 3). Although the Coriolis term is large (Table 1), it is not well correlated with any of the other terms. When the Coriolis term is added to the balances in Table 3, it does not improve the regression slopes. The large size of $f\overline{u}$

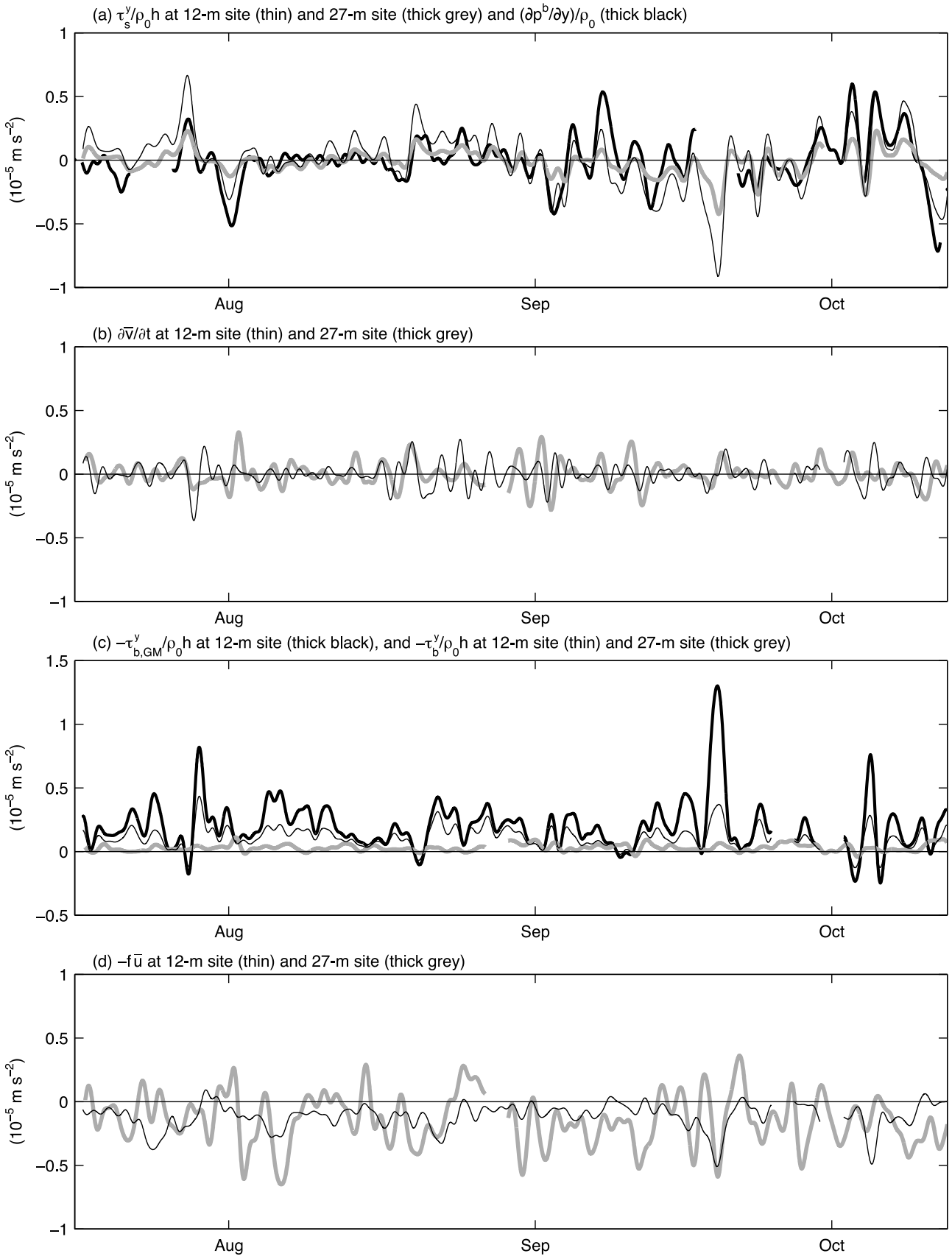

Figure 5. Dominant terms in the subtidal along-shelf momentum budget, CBLAST 2003.

Table 3. Regression Slope and Correlation Coefficient r of Terms in the Along-Shelf Momentum Budget at the Node and F Against the Along-Shelf Pressure Gradient $(\partial p^b/\partial y)/\rho_0$ With Zero Lag, for Times When All Terms are Available[a]

	Slope	r
12 m Water Depth		
$\frac{\tau_s^y}{\rho_0 h}$	0.9 ± 0.4	0.7
$\frac{\tau_s^y - \tau_b^y}{\rho_0 h}$	0.9 ± 0.5	0.7
$-\frac{\partial \overline{v}}{\partial t} + \frac{\tau_s^y - \tau_b^y}{\rho_0 h}$	1.0 ± 0.6	0.6
27 m Water Depth		
$\frac{\tau_s^y}{\rho_0 h}$	0.3 ± 0.2	0.7
$\frac{\tau_s^y - \tau_b^y}{\rho_0 h}$	0.7 ± 0.3	0.4
$-\frac{\partial \overline{v}}{\partial t} + \frac{\tau_s^y}{\rho_0 h}$	0.3 ± 0.3	0.4
$-\frac{\partial \overline{v}}{\partial t} + \frac{\tau_s^y - \tau_b^y}{\tau_0 h}$	0.3 ± 0.3	0.4

[a]Using GM bottom stress does not substantially change these results.

is not due to uncertainty in the coordinate system: only the mean value of $f\overline{u}$, not the standard deviation, is sensitive to rotating the coordinate system by ±5°. In previous studies, inaccuracies in the current meter measurements have been invoked to explain large values of $f\overline{u}$ [e.g., *Lentz et al.*, 1999]. The standard deviation of $\overline{u}$ at the 27 m site is 2 cm s^{-1} and the uncertainty in the ADCP velocities is ~1.5 cm s^{-1} [*Plueddemann et al.*, 2003]. There is a plausible dynamical explanation for the lack of correlation between $f\overline{u}$ and other terms. There could be cross-isobath flow at the 27 m site due to the nearby topographic variations (Figure 1) balanced by a small-scale (<10–15 km) unresolved pressure gradient. Supporting that idea, $f\overline{u}$ is weakly correlated with the along-shelf wind stress. The sign of the correlation is consistent with along-shelf wind causing cross-isobath flow due to the narrowing of the isobaths to the east (i.e., an eastward wind stress causing offshore flow throughout the water column at the 27 m site). There are two other indications that short spatial scales characterize the flow at the 27 m site: the along-shelf depth-average flows at the 12 and 27 m sites are not well correlated (r = 0.27 during SWWIM I and r = 0.58 during CBLAST 2003), and substantial along-shelf advective heat flux divergences are required to close the observed synoptic heat budget at that site [*Fewings*, 2007].

[34] In the time-mean balance, at the 12 m site the important terms are wind stress (in winter only), bottom stress, Coriolis, and Hasselmann wave stress. The Coriolis and Hasselmann wave stress terms tend to balance at this site due to a mean offshore flow associated with surface gravity wave forcing [*Lentz et al.*, 2008]. The sea level gradient required to close the time-mean budget at the 12 m site over all times is $\sim 1.8 \times 10^{-7}$, with sea level increasing eastward (independent of whether we use GM bottom stress). That is substantially larger than the along-shelf sea level gradient of 3.7×10^{-8} recently inferred for the Middle Atlantic Bight (the area between Cape Cod and Cape Hatteras) as a whole [*Lentz*, 2008] but similar to the inner shelf sea level gradients inferred in that study from wind stress and bottom stress alone, and similar to the 1.4×10^{-7} found for the inner shelf of Long Island [*Scott and Csanady*, 1976] and to studies in New Jersey [*Beardsley et al.*, 1977] and South Carolina [*Lee et al.*, 1989]. A small-scale sea level gradient that is large in magnitude compared to the mean sea level gradient along the Middle Atlantic Bight may be set up by the complex topography in the inshore ~10 km near MVCO during winter and spring. In summer the sea level gradient may be smaller, since the residual at the 12 m site is zero in summer if we do not use GM bottom stress.

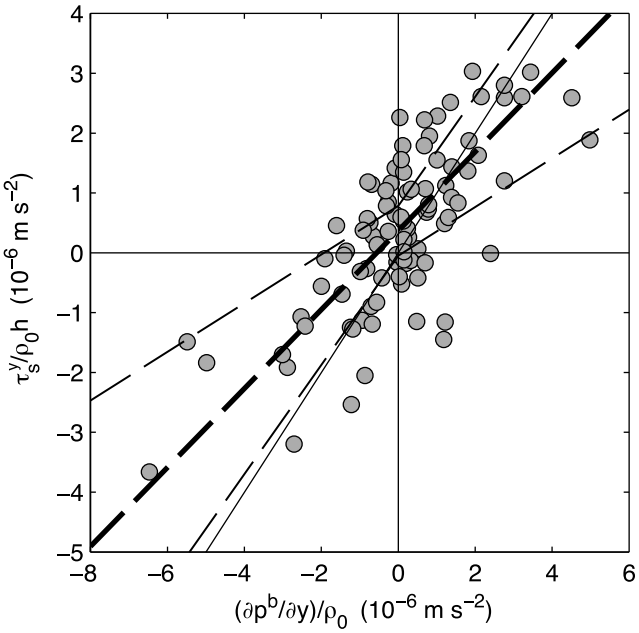

Figure 6. Comparison of wind stress and pressure gradient terms in the along-shelf momentum budget in 2001 (water depth 19 m) and 2003 (water depth 15 m) using wind stress in the Node coordinate system. Solid line has slope 1. For the combined data, the slope is 0.7 ± 0.3 and correlation is r = 0.7. See Table 4 for regression slope, intercept, and correlation coefficient for each year separately.

[35] At the 27 m site, the time-mean balance is dominated by the Coriolis term, and the sum of all the other terms closes the budget. No mean along-shelf sea level gradient is required. The difference in residual between the 12 and 27 m sites, which are only ~10 km apart, again suggests sea level gradients with small spatial scales (<10 km) are set up near MVCO due to the local topography.

5. Discussion

5.1. Horizontal Scales of the Pressure Gradient

[36] Interpretation of the across-shelf momentum balance depends on the across-shelf structure of the pressure field. If

Table 4. Regression and Correlation of Along-Shelf Wind Stress Term $\tau_s^y/\rho_0 h$ Versus Along-Shelf Pressure Gradient Term p_y^b/ρ_0, Using the Wind Stress in the 12 m Site Coordinate System at Zero Lag[a]

Year	Isobath	Slope	Intercept (10^{-6} m s^{-2})	Correlation Coefficient r
2001	19 m	1.4 ± 1.1	−1 ± 1	0.8
2003	15 m	1.1 ± 0.6	0.0 ± 0.1	0.7

[a]For h in the wind stress term, we use the isobath on which the pressure sensors were deployed.

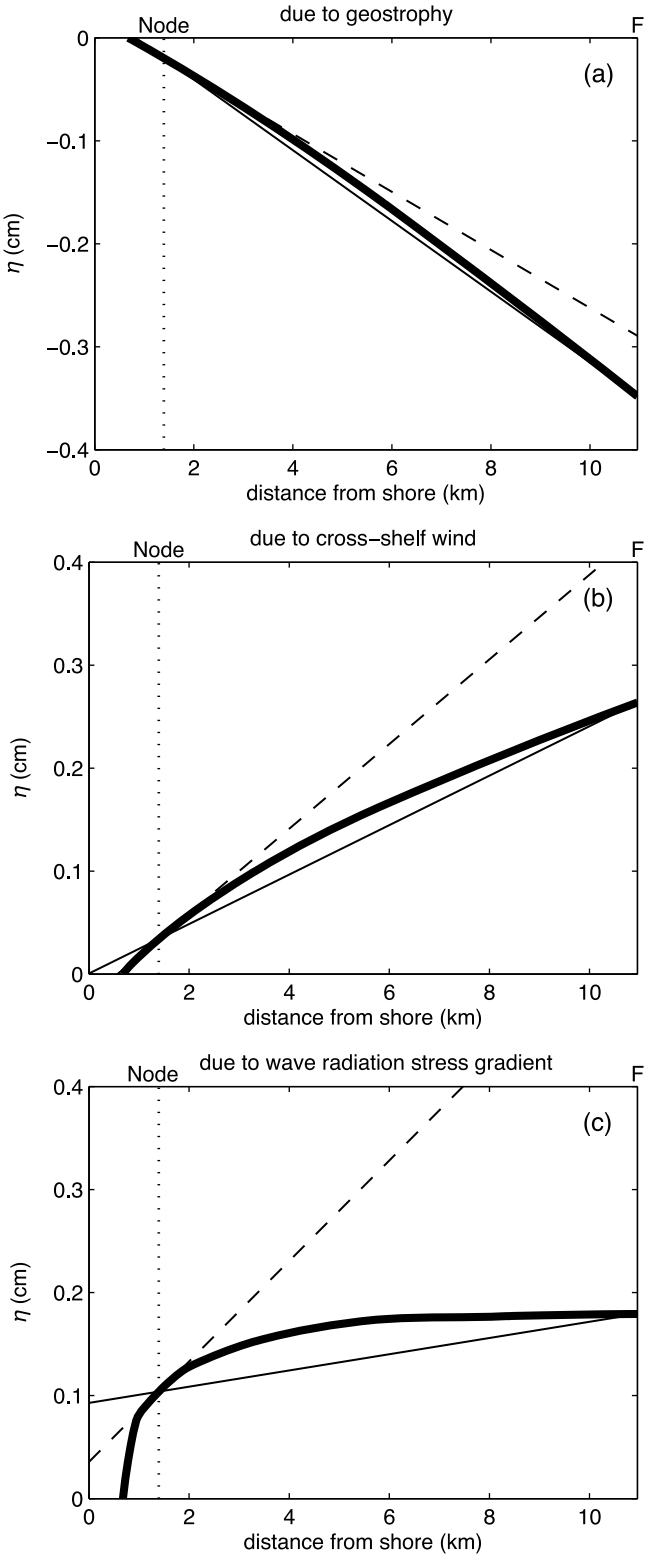

Figure 7. Across-shelf structure of sea level displacement η due to (a) geostrophy, (b) across-shelf wind, or (c) wave forcing. Thick line is η relative to its value at the 8 m isobath, from section 5.1. Thin line is the effective η profile for an observational pressure gradient estimate when p^b (or η) is measured at the Node and mooring F only. Dashed line is a least-squares fit to η near the Node (between 1.2 and 1.6 km from shore).

the distance over which dynamically important sea level variations take place is small compared to the distance between the pressure sensors used here (10–15 km), our pressure gradient estimates may be too small. The scale of across-shelf pressure gradient variation depends on whether the pressure gradient is due to geostrophic balance, coastal setup/setdown driven by the across-shelf wind, or coastal setdown driven by the wave radiation stress gradient. For each of those three cases, we use the hydrostatic relation and an integral in the across-shelf direction to calculate the sea level displacement η relative to its value at (for instance) the 8 m isobath, similarly to the method used by *Liu and Weisberg* [2007].

[37] If the across-shelf momentum balance is exactly geostrophic, then

$$\eta(x) - \eta|_{h=8\text{ m}} = \frac{f}{g}\int_{x|_{h=8\text{ m}}}^{x} \overline{v}\, dx' . \tag{7}$$

To estimate $\overline{v}$ at MVCO, we use the observed time-mean along-shelf flow in the Middle Atlantic Bight from *Lentz* [2008]: the flow increases linearly with water depth as

$$\overline{v} = \left(-0.065\text{ cm s}^{-1}\text{ m}^{-1}\right)h(x) - 2.1\text{ cm s}^{-1}. \tag{8}$$

The resulting sea level displacement is negative, and its magnitude increases with water depth (Figure 7a).

[38] If the across-shelf momentum budget is exactly a coastal setup/setdown balance between the across-shelf pressure gradient and a spatially uniform across-shelf wind stress, then

$$\eta(x) - \eta|_{h=8\text{ m}} = \frac{\tau_s^x}{\rho_0 g}\int_{x|_{h=8\text{ m}}}^{x} \frac{1}{h(x')}\, dx' . \tag{9}$$

For this example, we use $\tau_s^x = 0.05$ N m^{-2} and the MVCO bathymetry $h(x)$. The sea level displacement due to this moderate offshore wind forcing is positive and increases away from the coast: there is a coastal setdown (Figure 7b). In this model, for wind stress forcing of the opposite sign the sea level displacement would simply be opposite in sign (coastal setup).

[39] If the across-shelf momentum budget is exactly a coastal set down balance due to the across-shelf wave radiation stress gradient from shoaling waves, the sea level displacement relative to its value at the 8 m isobath is [see also *Longuet-Higgins and Stewart*, 1964]

$$\eta(x) - \eta|_{h=8\text{ m}} = -\frac{1}{\rho_0 g}\int_{x|_{h=8\text{ m}}}^{x} \frac{1}{h(x')}\frac{\partial S^{x'x'}}{\partial x'}\, dx' . \tag{10}$$

To estimate S^{xx} we use linear wave theory to find H_{sig} (x), assuming no dissipation of wave energy, for a wave propagating directly onshore with $H_{sig} = 1$ m at the 12 m isobath and a typical MVCO wave period of 6 s. The resulting sea level displacement is positive and increases rapidly from the 8 m isobath past the 12 m isobath before leveling off between the 12 and 27 m isobaths (Figure 7c).

[40] The sea level displacement due to geostrophic balance or across-shelf wind forcing grows approximately linearly with distance from shore over the entire region, assuming $\overline{v}$ has the form in equation (8) (Figures 7a and 7b). In contrast, the sea level displacement due to wave forcing does not

increase linearly with distance from shore (Figure 7c). As a result, the sea level gradient estimated from the bottom pressure difference between the 12 and 27 m sites may be a good proxy for the sea level gradient at those sites when the Coriolis term due to along-shelf flow or the across-shelf wind stress is the dominant forcing, but not when wave forcing is dominant. For example, at the 12 m site, the ratio of the true gradient to the estimated gradient is 0.8, 1.7, and 6.2 for the geostrophic, wind, and wave balances, respectively, so the pressure gradients discussed in section 4 could be underestimated by a factor of ~5–10 during wave forcing. This may be the reason for the lack of correlation of the estimated across-shelf pressure gradient and wave radiation stress gradient, in spite of the apparently large wave radiation stress gradient.

5.2. Sea Level Gradients

[41] The fluctuating along-shelf sea level gradients measured here are similar in size to gradients measured on the deeper continental shelf southwest of MVCO by *Beardsley et al.* [1977]. In that study, the along-shelf sea level gradients are 10 times smaller than the across-shelf gradients. In contrast, in this study the fluctuating along-shelf pressure gradient is only ~3 times smaller than the across-shelf gradient (Table 1), and the inferred mean across-shelf and along-shelf pressure gradients are similar in magnitude near the 12 m site. As discussed in sections 4.1 and 5.1, the fluctuating across-shelf sea level gradient may be an underestimate by a factor of 5–10 near the 12 m site during wave forcing, but that wave-forced gradient would be confined to water depths shallower than studied by *Beardsley et al.* [1977]. Possibly the across-shelf gradient is larger compared to the along-shelf gradient during winters, when no along-shelf gradient measurements were available.

5.3. Along-Shelf Flow and Wind Stress

[42] The along-shelf depth-average flow $\overline{v}$ is well correlated with the along-shelf wind stress τ_s^y on subtidal time scales, particularly at the 12 m site ($r = 0.8$, or $r = 0.6$ for times when the pressure gradient is available). A similar correlation exists at midshelf locations in the Middle Atlantic Bight and on other shallow shelves [*Shearman and Lentz*, 2003; *Mitchum and Sturges*, 1982; *Churchill*, 1985]. A linear relation between τ_s^y and $\overline{v}$ can be produced by the combined wind stress and pressure gradient forcing, as follows, if the bottom stress is linearly related to $\overline{v}$.

[43] The dominant along-shelf momentum balance at the 12 m site is between the wind stress, bottom stress, and pressure gradient (a three-term balance). If the bottom stress is related to the along-shelf velocity by the linear drag law $\tau_{b\,\mathrm{lin}}^y = \rho_0 r_b \overline{v}$, where r_b is the bottom drag coefficient, the three-term balance can be solved for the predicted along-shelf flow $\overline{v}_p$

$$\overline{v}_p = \frac{h}{\rho_0 r_b}\left(-\frac{\partial p^b}{\partial y} + \frac{\tau_s^y}{h}\right). \tag{11}$$

Because the pressure gradient and wind stress are linearly related (Table 4), $\overline{v}_p$ will be linearly related to the wind stress. Below, we compare $\overline{v}_p$ with the observed along-shelf flow at each site.

[44] Alternatively, we can take into account the acceleration term, which is not completely negligible (section 4.2), using a method from *Lentz and Winant* [1986]. Because the wind stress, bottom stress, and pressure gradient are not exactly in balance, the difference between those terms could act as forcing for the along-shelf flow, which would accelerate until the bottom stress became large enough to balance the wind stress and pressure gradient. The along-shelf momentum equation with acceleration (a four-term balance) is

$$\frac{\partial \overline{v}}{\partial t} + \frac{r_b \overline{v}}{h} = -\frac{1}{\rho_0}\frac{\partial p^b}{\partial y} + \frac{\tau_s^y}{\rho_0 h}, \tag{12}$$

The left-hand terms in equation (12) are the "response" to the right-hand "forcing" terms. The predicted along-shelf velocity $\overline{v}_p$ can be calculated by integrating equation (12) in time [*Lentz and Winant*, 1986] to get

$$\overline{v}_p = \int_{t_0}^{t}\left(-\frac{1}{\rho_0}\frac{\partial p^b}{\partial y} + \frac{\tau_s^y}{\rho_0 h}\right) e^{-(t-t')/T_f}\, dt' + \overline{v}|_{t=t_0}\, e^{-(t-t_0)/T_f}, \tag{13}$$

where $T_f \equiv (h/r_b)$ is the time scale over which bottom friction becomes important. If T_f is short compared to subtidal time scales (33 h), the response will be strongly affected by bottom friction and approximately steady [*Lentz et al.*, 1999]. For very short T_f, equation (11) based on the three-term balance should work as well as equation (13).

[45] At the 12 m site, a linear drag law fits the bottom stress well. The correlation of τ_b^y from section 3.1 with $\overline{v}$ is 0.95, and their regression slope gives a best-fit linear drag coefficient $r_b = 3.0 \pm 0.1 \times 10^{-4}$ m s^{-1}. If we regress $\overline{v}$ against $\tau_{b,GM}^y$, $r = 0.92$ and the linear drag coefficient is $5.5 \pm 0.2 \times 10^{-4}$ m s^{-1}. The regression method is explained in Appendix A. These drag coefficients are similar in magnitude to the value 2.5×10^{-4} m s^{-1} found for the Middle Atlantic Bight as a whole [*Lentz*, 2008]. The frictional time scale is short: $T_f = 11$ h (6 h for GM bottom stress).

[46] The steady, three-term balance (11) works as well as (13) at the 12 m site. During 2001, the correlation of $\overline{v}$ with $\overline{v}_p$ from (11) is $r = 0.8$ (Figure 8 (top)). The slope is 1.1, or 0.5 if we use GM bottom stress; this is the only case where using GM bottom stress makes the result worse. For 2003, when the pressure gradient is included (regardless of GM bottom stress, or three- versus four-way balance), the correlation of $\overline{v}$ with $\overline{v}_p$ is not significant at the 95% confidence level. In 2001 the results are always better (stronger correlation, and slope closer to 1) when pressure gradient is included, suggesting that although the pressure gradient is an important forcing term at the 12 m site, our measurements in 2003 are not accurate enough to be useful for a predictive model. Low-frequency drifts due to settling of the pressure sensors into the bottom that could not be perfectly removed from the pressure measurements may be adding low-frequency "noise" to $\overline{v}_p$ in 2003. If we calculate $\overline{v}_p$ without the pressure gradient, in 2003 the time-integrated model is marginally but not significantly better than the steady balance (Figure 8 (bottom)). The 12 m site, with a frictional time scale of 6–11 h, is in a regime where the adjustment time scale is short enough that a steady balance is a good approximation; acceleration is only marginally important. A balance between bottom stress, wind stress, and

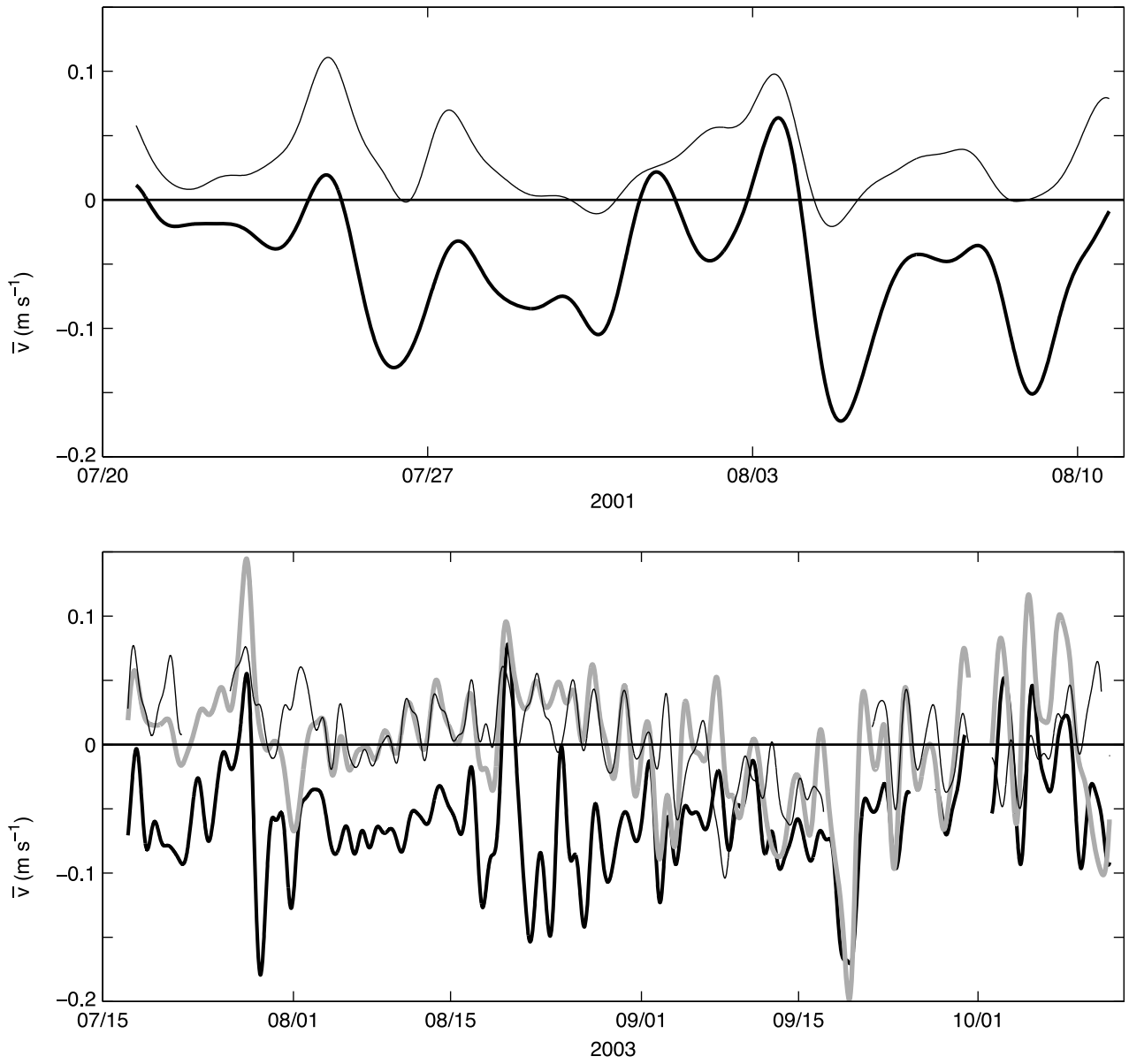

Figure 8. The 33 h low-pass filtered depth-average along-shelf flow $\overline{v}$ at the 12 m site in (top) 2001 and (bottom) 2003. Thick black line is observed $\overline{v}$. Thin line is predicted $\overline{v}_p$ from from a steady three-way balance between wind stress, GM bottom stress, and pressure gradient (section 5.3). Thick grey line in Figure 8 (bottom) is $\overline{v}_p$ from steady balance of wind and bottom stresses only, without pressure gradient.

pressure gradient (Figure 4d) is a plausible explanation for the strong relation between $\overline{v}$ and τ_s^y observed at the 12 m site.

[47] At the 27 m site, the models in equations (11) and (12) do not work well. The best-fit linear drag coefficient, $r_b = (1.3 \pm 0.1) \times 10^{-4}$ m s^{-1}, is smaller than at the shallower site, which combines with the larger water depth to make the frictional time scale much longer: $T_f = 60$ h. The $\overline{v}_p$ at the 27 m site (not shown) is not significantly correlated with the observed $\overline{v}$, suggesting the momentum balance at the 27 m site is not well represented by equation (12) due to the importance of $f\overline{u}$ and small-scale unresolved pressure gradients in the balance at that site.

5.4. Most Influential Wind Direction

[48] If the spatial scale of the wind stress field is large, the wind stress component that has the strongest effect on the local along-isobath flow may be parallel to the large-scale (~1000 km) coastline direction rather than the local along-isobath direction [*Allen*, 1980; *Beardsley et al.*, 1985; *Shearman and Lentz*, 2003]. At the Coastal Mixing and Optics site on the 70 m isobath south of MVCO, the wind direction most correlated with depth-average along-isobath flow is 65° counterclockwise from the local isobaths [*Shearman and Lentz*, 2003] and parallel to the coastline orientation on large (>1000 km) scales [*Noble and Butman*, 1983; *Shearman*

and Lentz, 2003]. In the MVCO area, however, the wind stress component most highly correlated with the along-shelf pressure gradient and the along-shelf depth-average flow is within 15° of the local along-shelf principal axis direction for both the 12 and 27 m sites, and parallels the coastline orientation calculated on smaller scales of 100–200 km by *Shearman and Lentz* [2003]. Close to shore near MVCO, the small-scale (~100 km) coastline orientation is the wind direction most relevant for along-shelf flow dynamics.

6. Summary and Conclusions

[49] The subtidal fluctuating depth-average across-shelf momentum budget over the inner continental shelf at two sites near MVCO is not simply geostrophic, as would be expected at midshelf. The observed across-shelf momentum budget closes best if the across-shelf wind stress, pressure gradient, and Coriolis terms are included (Figures 2e, 3, 4a, and 4b). At the site on the 12 m isobath, the calculated wave radiation stress gradient is also large but it is not correlated with the across-shelf pressure gradient, in contrast to what is expected for setdown due to shoaling waves outside the surfzone [*Longuet-Higgins and Stewart*, 1964; *Bowen et al.*, 1968; *Lentz et al.*, 1999; *Raubenheimer et al.*, 2001] (Figure 4c). Either the true wave radiation stress gradient is smaller than our estimate or, in agreement with a simple model (section 5.1), the wave radiation stress is balanced by a pressure gradient with a smaller across-shelf scale than is resolved by these observations (Figure 7).

[50] In the fluctuating along-shelf momentum balance, the dominant terms are wind stress and pressure gradient, plus bottom stress at the 12 m site and Coriolis acceleration due to across-shelf flow at the 27 m site (Figures 5a, 5c, 5d, and 4d). The budget with those terms closes at the 12 m but not the 27 m site, where the Coriolis term may be balanced by unresolved small-scale pressure gradients. The acceleration is not negligible in size at either site, but does not significantly improve the closure. The pressure gradient is largely a local sea level response to wind forcing rather than a remotely generated pressure gradient. The *Grant and Madsen* [1986] model of wave-enhanced bottom stress substantially improves the regression slope between surface and bottom stress at the 12 m site in winter, lending support to that model of wave-current interaction.

[51] The time-mean across-shelf budget at the 12 m site is dominated by the wave radiation stress gradient and the Coriolis term due to along-shelf flow, suggesting a combined wave setdown and geostrophic balance with a mean along-shelf pressure gradient. The across-shelf budget at the 27 m site is dominated by Coriolis, suggesting a mean geostrophic balance between the along-shelf flow and an along-shelf pressure gradient. The residuals in the time-mean budgets suggest mean sea level gradients of $O(5 \times 10^{-7})$ in the across-shelf direction and $O(2 \times 10^{-7})$ in the along-shelf direction (sea level increasing eastward) exist in the MVCO area.

[52] The wind stress direction most correlated with the depth-average subtidal along-shelf flow at both sites is within 15° of the local isobath direction, and similar to the small-scale (100–200 km) coastline orientation calculated by *Shearman and Lentz* [2003] for this area. There is a strong correlation between the along-shelf depth-average flow and the along-shelf wind stress at the 12 m site. The along-shelf flow predicted by a steady balance between wind stress, along-shelf pressure gradient, and a linear bottom drag is similarly correlated with the wind stress. At the 27 m site that simple model is not successful at predicting the along-shelf flow, consistent with other evidence that the two sites are in regions with different dynamics.

[53] Dynamically important sea level gradients with horizontal scales too small to resolve with these observations seem to exist in both the along-shelf and across-shelf directions and could be captured in future studies. The measurements of along-shelf pressure gradient available for this study were mainly collected during summer, when the wind forcing and wave forcing are relatively weak. Measurements of the along-shelf pressure gradient during strong winter forcing would better test these balances and help to determine which secondary terms in the along-shelf momentum budget are the most important. The wave radiation stress gradient and the amount of wave dissipation over the inner shelf are also very uncertain, and could be estimated more accurately by recording the directional wave spectrum at several sites in an across-shelf transect. The nonlinear advection terms, though not resolved here, are potentially not negligible and their importance over the inner shelf, where flow speeds tend to decrease approaching the coast, should be determined. It will be important in future inner shelf studies to have measurements with finer spatial resolution of the gradients in pressure, wave characteristics, and water velocities.

Appendix A: Regression Technique and Uncertainties in Momentum Budget Terms

[54] To calculate linear regressions while allowing for measurement uncertainty in both the independent and dependent variables, we used the "weighted total least squares" algorithm of *Krystek and Anton* [2007]. We estimate the uncertainty in the ADCP velocities as $\delta u = 0.015$ m s^{-1} [*Plueddemann et al.*, 2003]. The estimated uncertainties in density and pressure gradients, wind stress, wave radiation stress gradient, vertical shear, and acceleration and Coriolis terms are described by *Fewings* [2007].

[55] The uncertainty in the Hasselmann wave stress terms of equations (1) and (2) is due to uncertainty in the observed water velocity spectrum from which the wave parameters are calculated. Because the Hasselmann wave stress is not a dominant term in either fluctuating momentum budget, the uncertainty we assume does not affect our results and we simply use an uncertainty of 50%.

[56] The fractional uncertainty in the across-shelf bottom stress component was estimated as

$$\frac{\delta\tau_b^x}{|\tau_b^x|} = \sqrt{\left(\frac{\delta C_d}{C_d}\right)^2 + \left(\frac{\delta u}{\sigma(|\mathbf{u_b}|)}\right)^2 + \left(\frac{\delta u}{\sigma(|u_b|)}\right)^2}, \qquad \text{(A1)}$$

where σ indicates standard deviation, used to avoid problems with near-zero values of u_b in the denominator. We use $\delta C_d/C_d \sim 0.16$, which is based on a regression of direct

covariance measurements of $\langle u'_a w' \rangle$ against measured $u_a|\mathbf{u}_a|$, where primes indicate turbulent velocity fluctuations, angle brackets indicate an average over time scales long compared to the turbulent time scales, and subscript a indicates along-stream velocity (J. Trowbridge, personal communication, 2009). For along-shelf bottom stress, v_b is substituted for u_b in the last term of equation (A1). The resulting fractional uncertainties at the Node (F) are 0.51 (0.43) in the across-shelf and 0.28 (0.34) in the along-shelf direction.

[57] **Acknowledgments.** We thank Robert Beardsley, Glenn Flierl, Heidi Sosik, Glen Gawarkiewicz, Melissa Moulton, and two anonymous reviewers for helpful comments on this manuscript. Eugene Terray provided helpful discussion of the uncertainties in surface wave parameters from ADCP velocities. Carlos Moffat provided some MATLAB scripts. We thank Robert Weller and John Trowbridge for providing mooring data from CBLAST 2003. We also thank Tom Farrar, Robert Weller, Jim Lerczak, and Jay Sisson for deployment of the CBLAST F ADCP; the captain and crew of the R/V *Connecticut* for mooring recovery in fall 2003; Janet Fredericks and Craig Marquette for data downloading; and Craig Marquette, Jim Dunn, Jeff Lord, Scott Worrilow, John Lund, Rick Rupan, Carlos Moffat, Jessica Warren, Clare Williams, and especially Captain Ken Houtler and crew member Ian Hanley of R/V *Tioga* for deployment and recovery of the SWWIM I moorings. This research was funded by the Ocean Sciences Division of the National Science Foundation under grants OCE-0241292 and OCE-0548961 and by the National Aeronautics and Space Administration Headquarters under grant NNG04GL03G and the Earth System Science Fellowship grant NNG04GQ14H. MVCO is partly funded by the Woods Hole Oceanographic Institution and the Jewett/EDUC/Harrison Foundation. CBLAST 2003 was funded by the Office of Naval Research contracts N00014-01-1-0029 and N00014-05-10090 for the Low-Wind Component of the Coupled Boundary Layers Air-Sea Transfer Experiment. The F ADCP, T1 and T2 moorings, and temperature measurements near the Node in 2003 were funded by the National Science Foundation Small Grant for Exploratory Research OCE-0337892 ("Observational Mesoscale Context for Oceanic Turbulence Measurements Obtained during CBLAST-Low").

References

Allen, J. S. (1980), Models of wind-driven currents on the continental shelf, *Annu. Rev. Fluid Mech.*, *12*, 389–433.

Allen, J. S., and P. K. Kundu (1978), On the momentum, vorticity, and mass balance on the Oregon shelf, *J. Phys. Oceanogr.*, *8*, 13–27.

Allen, J. S., and R. L. Smith (1981), On the dynamics of wind-driven shelf currents, *Philos. Trans. R. Soc. London A*, *302*, 617–634.

Beardsley, R. C., H. Mofjeld, M. Wimbush, C. N. Flagg, and J. A. Vermersch (1977), Ocean tides and weather-induced bottom pressure fluctuations in the Middle-Atlantic Bight, *J. Geophys. Res.*, *82*, 3175–3182.

Beardsley, R. C., D. C. Chapman, K. H. Brink, S. R. Ramp, and R. Schlitz (1985), The Nantucket Shoals Flux Experiment (NSFE79). Part I: A basic description of the current and temperature variability, *J. Phys. Oceanogr.*, *15*, 713–748.

Blanton, J. O. (1981), Ocean currents along a nearshore frontal zone on the continental shelf of the southeastern United States, *J. Phys. Oceanogr.*, *11*, 1627–1637.

Bowen, A. J., D. L. Inman, and V. P. Simmons (1968), Wave "set-down" and set-up, *J. Geophys. Res.*, *73*, 2569–2577.

Brown, W. S., N. R. Pettigrew, and J. D. Irish (1985), The Nantucket Shoals Flux Experiment (NSFE79). Part II: The structure and variability of across-shelf pressure gradients, *J. Phys. Oceanogr.*, *15*, 749–771.

Brown, W. S., J. D. Irish, and C. D. Winant (1987), A description of subtidal pressure field observations on the northern California continental shelf during the Coastal Ocean Dynamics Experiment, *J. Geophys. Res.*, *92*, 1605–1636.

Churchill, J. H. (1985), Properties of flow within the coastal boundary layer off Long Island, New York, *J. Phys. Oceanogr.*, *15*, 898–916.

Feddersen, F., R. T. Guza, S. Elgar, and T. H. C. Herbers (1998), Alongshore momentum balances in the nearshore, *J. Geophys. Res.*, *103*, 15,667–15,676.

Fewings, M. R. (2007), Cross-shelf circulation and momentum and heat balances over the inner continental shelf near Martha's Vineyard, Massachusetts, Ph.D. thesis, 267 pp., MIT/WHOI Jt. Program in Oceanogr./Appl. Ocean Sci. and Eng., Woods Hole, Mass. (Available at http://hdl.handle.net/1912/2121.)

Fewings, M. R., S. J. Lentz, and J. Fredericks (2008), Observations of cross-shelf flow driven by cross-shelf winds over the inner continental shelf, *J. Phys. Oceanogr.*, *38*, 2358–2378.

Grant, W., and O. Madsen (1979), Combined wave and current interaction with a rough bottom, *J. Geophys. Res.*, *84*, 1797–1808.

Grant, W., and O. Madsen (1986), The continental-shelf bottom boundary layer, *Annu. Rev. Fluid Mech.*, *18*, 265–305.

Hasselmann, K. (1970), Wave-driven inertial oscillations, *Geophys. Fluid Dyn.*, *1*, 463–502.

Kirincich, A., S. J. Lentz, and G. P. Gerbi (2010), Calculating Reynolds stresses from ADCP measurements in the presence of surface gravity waves using the cospectra-fit method, *J. Atmos. Oceanic Technol.*, *27*, 889–890, doi:10.1175/2009JTECHO682.1.

Krystek, M., and M. Anton (2007), A weighted total least-squares algorithm for fitting a straight line, *Meas. Sci. Technol.*, *18*, 3438–3442.

Lee, T. N., W. J. Ho, V. Kourafalou, and J. D. Wang (1984), Circulation on the continental shelf of the southeastern United States. Part I: Subtidal response to wind and Gulf Stream forcing during winter, *J. Phys. Oceanogr.*, *14*, 1001–1012.

Lee, T. N., E. Williams, R. E. J. Wang, and L. Atkinson (1989), Response of South Carolina continental shelf waters to wind and Gulf Stream forcing during winter of 1986, *J. Geophys. Res.*, *94*, 10,715–10,754.

Lentz, S. J. (1994), Current dynamics over the northern California inner shelf, *J. Phys. Oceanogr.*, *24*, 2461–2478.

Lentz, S. J. (1995), Sensitivity of the inner-shelf circulation to the form of the eddy viscosity profile, *J. Phys. Oceanogr.*, *25*, 19–28.

Lentz, S. J. (2008), Observations and a model of the mean circulation over the Middle Atlantic Bight continental shelf, *J. Phys. Oceanogr.*, *38*, 1203–1221.

Lentz, S. J., and B. Raubenheimer (1999), Field observations of wave setup, *J. Geophys. Res.*, *104*, 25,867–25,875.

Lentz, S. J., and C. D. Winant (1986), Subinertial currents on the southern California shelf, *J. Phys. Oceanogr.*, *16*, 1737–1750.

Lentz, S. J., R. T. Guza, S. Elgar, F. Feddersen, and T. H. C. Herbers (1999), Momentum balances on the North Carolina inner shelf, *J. Geophys. Res.*, *104*, 18,205–18,226.

Lentz, S. J., M. R. Fewings, P. Howd, J. Fredericks, and K. Hathaway (2008), Observations and a model of undertow over the inner continental shelf, *J. Phys. Oceanogr.*, *38*, 2341–2357.

Li, Z., and R. H. Weisberg (1999a), West Florida shelf response to upwelling favorable wind forcing: Kinematics, *J. Geophys. Res.*, *104*, 13,507–13,527.

Li, Z., and R. H. Weisberg (1999b), West Florida continental shelf response to upwelling favorable wind forcing 2. Dynamics, *J. Geophys. Res.*, *104*, 23,427–23,442.

Liu, Y., and R. H. Weisberg (2005), Momentum balance diagnoses for the West Florida Shelf, *Cont. Shelf Res.*, *25*, 2054–2074.

Liu, Y., and R. H. Weisberg (2007), Ocean currents and sea surface heights estimated across the west Florida shelf, *J. Phys. Oceanogr.*, *37*, 1697–1713.

Longuet-Higgins, M. S. (1953), Mass transport in water waves, *Philos. Trans. R. Soc. London A*, *245*, 535–581.

Longuet-Higgins, M. S., and R. W. Stewart (1964), Radiation stresses in water waves; a physical discussion, with applications, *Deep Sea Res. Oceanogr. Abstr.*, *11*, 529–562.

Masse, A. (1988), Estuary-shelf interaction: Delaware Bay and the inner shelf, Ph.D. thesis, Univ. of Del., Newark, Del.

Mitchum, G., and W. Sturges (1982), Wind-driven currents on the west Florida shelf, *J. Phys. Oceanogr.*, *12*, 1310–1317.

Noble, M., and B. Butman (1983), On the longshelf structure and dynamics of subtidal currents on the eastern United States continental shelf, *J. Phys. Oceanogr.*, *13*, 2125–2146.

Pettigrew, N. R. (1981), The dynamics and kinematics of the coastal boundary layer off Long Island, Ph.D. thesis, Woods Hole Oceanogr. Inst., Woods Hole, Mass.

Plueddemann, A. J., S. J. Lentz, and E. A. Terray (2003), Comparison of five current meters in a tidally dominated flow, in *Proceedings of the IEEE/OES Seventh Working Conference on Current Measurement Technology*, pp. 176–181, Inst. of Electr. and Electr. Eng., Piscataway, N. J.

Raubenheimer, B., R. T. Guza, and S. Elgar (2001), Field observations of wave-driven setdown and setup, *J. Geophys. Res.*, *106*, 4629–4638.

Scott, J. T., and G. T. Csanady (1976), Nearshore currents off Long Island, *J. Geophys. Res.*, *81*, 5401–5402.

Shearman, K., and S. J. Lentz (2003), Dynamics of mean and subtidal flow on the New England shelf, *J. Geophys. Res.*, *108*(C8), 3281, doi:10.1029/2002JC001417.

Smith, S. D. (1988), Coefficients for sea surface wind stress, heat flux, and wind profiles as a function of wind speed and temperature, *J. Geophys. Res.*, *93*, 15,467–15,472.

Stokes, G. G. (1847), On the theory of oscillatory waves, *Trans. Cambridge Philos. Soc.*, *8*, 441–455.

Svendsen, I. A., and U. Putrevu (1994), Nearshore mixing and dispersion, *Proc. R. Soc. London A*, *445*, 561–576.

Thompson, K. R., and D. T. Pugh (1986), The subtidal behavior of the Celtic Sea—Part II. Currents, *Cont. Shelf Res.*, *5*, 321–346.

Thornton, E. B., and R. T. Guza (1986), Surf zone longshore currents and random waves: Field data and models, *J. Phys. Oceanogr.*, *16*, 1165–1178.

Tilburg, C. E. (2003), Across-shelf transport on a continental shelf: Do across-shelf winds matter?, *J. Phys. Oceanogr.*, *33*, 2675–2688.

Weisberg, R. H., Z. Li, and F. Muller-Karger (2001), West Florida shelf response to local wind forcing: April 1998, *J. Geophys. Res.*, *106*, 31,239–31,262.

Xu, Z., and A. J. Bowen (1994), Wave- and wind-driven flow in water of finite depth, *J. Phys. Oceanogr.*, *24*, 1850–1866.

M. R. Fewings, Marine Science Institute, University of California, Santa Barbara, Mail Code 6150, Santa Barbara, CA 93106-6150, USA. (fewings@msi.ucsb.edu)

S. J. Lentz, Department of Physical Oceanography, Woods Hole Oceanographic Institution, MS 21, Woods Hole, MA 02543, USA. (slentz@whoi.edu)